https://doi.org/10.1016/j.nanoen.2021.105814

Fully self-powered instantaneous wireless humidity sensing system based on triboelectric nanogenerator

Liangquan Xu,[1] Weipeng Xuan,[1*] Jinkai Chen,[1] Chi Zhang,[1] Yuzhi Tang,[1] Xiwei Huang,[1] Wenjun Li,[1] Hao Jin,[2] Shurong Dong,[2] Wuliang Yin,[3] Yongqing Fu,[4] Jikui Luo[2,1*]

1. *Ministry of Education Key Lab. of RF Circuits and Systems, College of Electronics & Information Hangzhou Dianzi University, Hangzhou, China.*
2. *Key Lab. of Adv. Micro/Nano Electron. Dev. & Smart Sys. of Zhejiang, College of Info. Sci. & Electron. Eng., Zhejiang University, Hangzhou, China.*
3. *School of Electrical and Electronic Engineering, University of Manchester, Manchester M13 9PL, UK*
4. *Faculty of Engineering and Environment, Northumbria University, Newcastle upon Tyne, NE1 8ST, UK*

Abstract: Self-powered wireless sensor systems are highly sorted for the forthcoming Internet of Things era. However, most of the technologies take the route of energy harvesting, storage, and power regulation to power wireless sensor systems, which has a limited operation duration due to the low energy utilization efficiency of the multiple energy conversions involved. Here, we propose a triboelectric nanogenerator (TENG) based fully self-powered, instantaneous wireless sensor system which yet does not contain electronic devices and chips, but the passive components only. By integrating a capacitive sensor and an inductor with TENG, the pulse voltage output of the TENG is converted into a sinusoidal signal containing the sensing information with a resonant frequency and is transmitted to the receiver in distance wirelessly and continuously. A precise analytical model is developed for the capacitive sensor system with general implication; the oscillating signal generated by the model shows excellent agreement with experimental results. A capacitive humidity sensor is then utilized for sensing demonstration, showing that the maximum transmission distance of the sensor system is 50 and 90 cm for a 1cm diameter magnetic-core coil pair and 20 cm diameter air-core coil pair, respectively. The wireless humidity sensor exhibits a sensitivity of 1.26 kHz/%RH, fast response speed, and excellent

linearity, demonstrated its great application potential of the self-powered technology.

Keywords: triboelectric nanogenerator; self-powered, instantaneous sensing, wireless and chipless sensor;

The corresponding authors email address: xuanweipeng@hdu.edu.cn, jackluo@zju.edu.cn

1. Introduction

The rapid development of the Internet of Things (IoT) and artificial intelligence (AI) has imposed great impacts on our daily lives, social activities, manufacturing and environmental protection etc. Wireless sensor networks (WSN) are one of the foundations of these advanced technologies[1-4]. Microsensors are playing an increasingly important role in modern society with widespread applications such as for smart manufacturing, smart home/city, ecological and environmental protection and disaster monitoring/controlling etc. Currently, the most commonly used environmental sensors include temperature and humidity sensors for air and soil quality monitoring, pressure sensors, chemical sensors for pollution monitoring etc.[5-9]. These sensors are typically wireless sensors, so that they can be deployed/distributed in remote/harsh environments to perform continuous monitoring function wirelessly[10-14]. The sensor networks normally are composed of multiple electronic devices and chip modules including analogue-digital (AD) converters, signal processing unit, power regulator modules, wireless transmission module etc. and of course the sensors[15]. They need electricity to power the sensors and electronic devices/chips, and batteries are the choice of power sources for these sensor networks. These not only require a lot of resources for periodical replacement of batteries before the end of their lifespan, but also cause environmental pollution by the waste batteries. These are not in line with the current trend of green and sustainable development.

The new concept is to develop sensor network systems that are able to collect environmental energy to power the systems themselves, realizing self-powered wireless sensing[16-22]. However, these types of self-power sensor systems need to harvest energy, store it in an energy storage device and then to power the wireless sensor system via voltage regulator modules. It involves multiple energy conversion routines, i.e. harvesting-storage-supplying, making the final energy utilization efficiency very low. It requires a long period of pre-operation to store sufficient energy before it can power the sensors and electronics,

especially the wireless transmission modules, for a very short period[23-27]. The sensor systems are in sleeping mode for majority of the operation time[28], thus the sensed and transmitted signals are not continuous and instantaneous, with the latter particularly important for crisis and accident monitoring such as bridge damage, flood etc.

The latest development for self-powered wireless sensor networks is to directly convert the energy of sensing variables into signals and transmit them wirelessly to the receiver side, with no or very little electronic devices involved as they require energy to operate. This enables continuous and instantaneous sensing without losing any sensing information. Recently, we developed fully self-powered sensor systems, which are able to perform sensing as well as transmitting power wirelessly instantaneously, either by light or by radio frequency (RF)[29, 30]. The sensor systems have utilized the newly developed triboelectric nanogenerators (TENG) [31-34] as the power sources, as well as the sensors. For the RF wireless sensing system, it is based on a magnetic resonance signal transmission, with either the TENG as a sensor or the sensor integrated into the resonance circuit of the system. Any variation of sensing parameters of the sensors would modulate the resonant frequency of the resonant circuit and the signal can be wirelessly transmitted through the magnetic resonance-coupled inductor coils. Since there is no energy storage and power regulation processes involved, this type of sensor systems has very high energy utilization efficiency, instantaneous sensing and signal transmission capability, yet has no additional electronic devices/chips but the passive capacitors and coils.

This work reports a further development of the TENG-based instantaneous, wireless and chipless humidity sensor system. An equivalent circuit model is developed for the sensor system which significantly simplifies the design of relevant sensor systems suitable for general applications. Based on the theoretical model and by utilizing a small ferric magnetic core for the transmission coils, a fully self-powered wireless humidity sensor system with much reduced coil dimension and longer transmission distance is obtained. The humidity sensor has high sensitivity, fast response and excellent linearity, demonstrated its great potential for practical application.

2. Results

2.1 Configuration of the wireless sensor system

In this section, we try to develop a circuit model for the TENG-based self-powered instantaneous wireless sensor systems suitable for general purposes and applications, i.e. for different types of sensing. **Fig. 1a** shows the schematic configuration of the wireless sensor system which, in principle, is similar to what was proposed in our previous work[29, 30]. It

consists of a TENG integrated with a synchronized microswitch, an L_1C_1 resonant circuit-based transmitter and an L_2C_2 resonant circuit-based receiver. L_1 and L_2 are coils for wireless signal transmission, C_1 is the capacitance of the capacitive sensor which could be any type of sensors such as humidity sensor in this work, vibration sensor or force sensor etc., C_2 is a tunable capacitance on the receiver side, and R_L is the load resistance of the receiver. The so-called chipless sensor system means that the system contains no additional electronic devices and transmission modules (chips), but the passive components of coils and capacitors. The working principle of the sensor system is as follows: when the TENG is stimulated by an external force such as mechanical vibration, wind etc, a voltage pulse is produced and coupled to the L_1C_1 resonant circuit, generating an oscillating signal with an attenuating amplitude[29]. Once the system is tuned in resonance, the oscillating signal containing sensing information can be transmitted wirelessly to the receiver in distance, realizing wireless sensing. To increase the signal amplitude, hence the transmission distance, a microswitch is utilized for the TENG system, which can increase the amplitude of TENG output voltage significantly[35, 36].

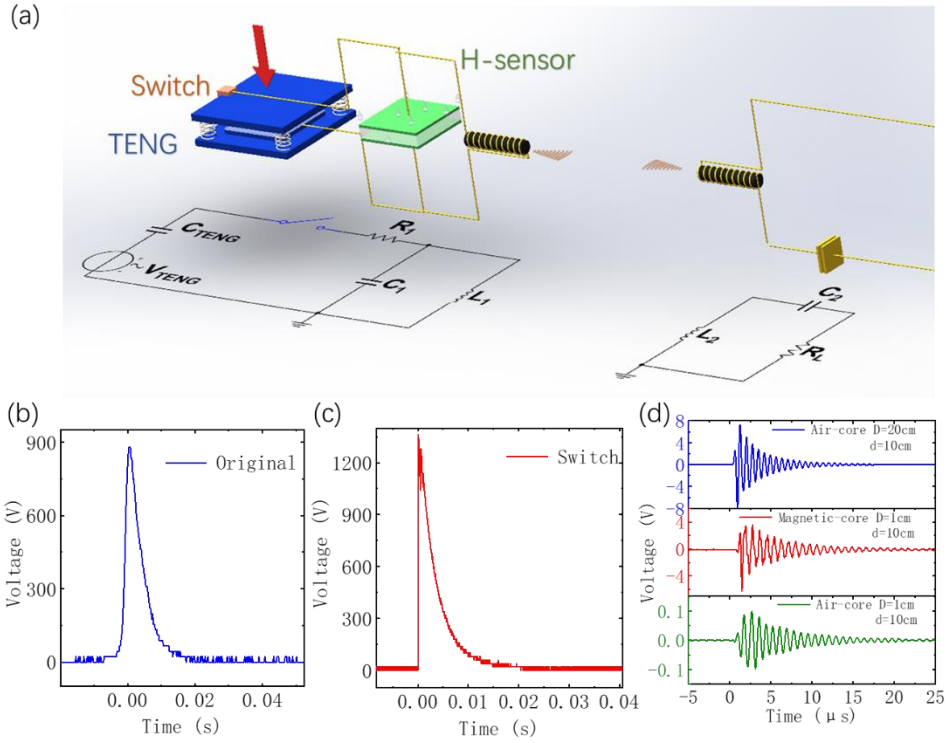

Fig. 1. (a) Schematic diagram of the TENG based self-powered wireless sensor system, (b) typical voltage output of a TENG, (c) typical voltage output of a TENG integrated with a synchronization microswitch, and (d) typical received signals when different types of coils are used at the same transmission distance.

Fig. 1b is a typical output of a TENG and **Fig. 1c** is an output of a TENG integrated with

a microswitch, showing a much-increased amplitude of the output voltage owing to the much-reduced discharging time as will be explained later. **Fig. 1d** shows the typical received signals when different types of coils are used with different transmission distances between the two coils. From our previous work, it is understood that the coupling coefficient between the two coils is the determinant factor affecting the wireless transmission distance of the signal. When the diameter of the coils becomes small, the transmission signal becomes weak drastically due to the reduced coupling coefficient. To increase the wireless transmission distance and decrease the dimensions of the system, small coils with a magnetic core are considered in this work as the magnetic core of the coils could increase the coupling coefficient drastically, hence to increase the transmission distance.

2.2 Theoretical analysis of WS-TENG

To derive an equivalent circuit and analytical formulas for the TENG-based self-powered wireless sensor system (WS-TENG), theoretical analysis was conducted which then can be used in much broader areas with general implication. It is well known that a TENG can be equivalent to a variable voltage source and a variable capacitor in series connection. The voltage output can be expressed by equ.(1) [37],

$$V_{TENG} = x(t)\frac{\sigma}{\varepsilon} \tag{1}$$

here σ is the surface charge density of the tribo-materials, ε is the vacuum dielectric constant, and $x(t)$ is the distance between the two tribo-material plates which varies with time during operation. The variable capacitance of the TENG is shown in equ.(2),

$$C_{TENG} = \frac{\varepsilon S}{d_0 + x(t)} \tag{2}$$

where d_0 is the thickness of the dielectric material, and S is the active contact area of the tribo-materials. The equivalent circuit of the wireless sensor system is shown in **Fig. 1a**. As mentioned above, to increase the output voltage signal amplitude, a synchronization microswitch was integrated into the system, which allows the instantaneous discharge of the accumulated charges on the surfaces of the tribo-materials[29, 30], that are generated through the combined effects of electrification and electrostatic induction[38]. The output voltage of TENG with a microswitch, V_S, is the discharge curve of a capacitor with time, thus it could be expressed as equ.(3), where τ is the attenuation factor of the output voltage, and U_0 is the output peak voltage.

$$V_S = U_0 e^{-\tau t} \tag{3}$$

From electronics point of view, it is known that the signal coupling between two coils can be treated as a T-shaped circuitry element with a mutual inductance, M, thus an equivalent circuit can be obtained for the wireless sensor system as shown in **Fig. 2a**, where L_1'=L_1-M, and L_2'=L_2-M. The receiver side can be represented by the circuit circulated by the dashed blue line as shown in **Fig. 2a**, and its output impedance, Z_{22}, is expressed by equ.(4).

$$Z_{22} = jw\,M\,//\,(jwL_2' + \frac{1}{jwC_2} + R_L) \tag{4}$$

Z_{22} is the impedance of the mutual inductance in parallel with the impedance of the receiver RLC circuit. Since the mutual inductance value M is very small for the wireless sensor system. Z_{22} can be simplified further as shown in equ.(5) and (6), respectively.

$$jwM << (jwL_2' + \frac{1}{jwC_2} + R_L) \tag{5}$$

$$Z_{22} \approx jwM \tag{6}$$

Assume V_1 is the voltage applied across capacitor C_1, and V_2 is the voltage applied across Z_{22}, via Laplace analysis on the simplified circuit diagram and setting $Z_{22}=Ms$, we obtain equ.(7) and (8).

$$V_1(s) = \frac{(AL_1'+AM)s}{(C_1L_1'R_1+C_1MR_1)s^3+(L_1'+M+C_1L_1'R_1\tau+C_1MR_1\tau)s^2+(R_1+L_1'\tau+M\tau)s+R_1\tau} \tag{7}$$

$$V_2(s) = \frac{(AM)s}{(C_1L_1'R_1+C_1MR_1)s^3+(L_1'+M+C_1L_1'R_1\tau+C_1MR_1\tau)s^2+(R_1+L_1'\tau+M\tau)s+R_1\tau} \tag{8}$$

Perform the inverse Laplace transform for $V_2(s)$, a time-domain voltage expression can be obtained as follows.

$$v_2(t) = Ae^{-at}(k_1\cosh(w_1t) + k_2\sinh(w_2t)) - k_3e^{-\tau t} \tag{9}$$

where A, a, k_1, k_2, k_3 and w_1 are defined as follows

$$A = \frac{(AC_1R_1\tau M^2 + AC_1L_1'R_1\tau M)}{(C_1L_1'R_1 + C_1MR_1)(R_1 - L_1'\tau - M\tau + C_1L_1'R_1\tau^2 + C_1MR_1\tau^2)}$$

$$a = \frac{(L_1' + M)}{2C_1L_1'R_1 + 2C_1MR_1}$$

$$k_1 = 1; k_2 = \frac{C_1R_1\left(\frac{L_1' + M}{2C_1L_1'R_1 + 2C_1MR_1} - \frac{AMR_1}{AC_1R_1\tau M^2 + AC_1L_1'R_1\tau M}\right)\sqrt{L_1' + M}}{\sqrt{-C_1{R_1}^2 + \frac{L_1'}{4} + \frac{M}{4}}}$$

$$k_3 = \frac{AM\tau}{R_1 - L_1'\tau - M\tau + C_1L_1'R_1\tau^2 + C_1MR_1\tau^2}$$

$$w_1 = w_2 = \frac{\sqrt{-C_1R_1^2 + \frac{L_1'}{4} + \frac{M}{4}}}{C_1R_1\sqrt{L_1' + M}}$$

Since V_2 is the voltage across the mutual inductance M, thus the receiver terminal can be further simplified into a circuit as shown by **Fig. 2b**. The voltage on the load resistance R_L can be easily obtained by a voltage divider and Laplace transform as formula (10), and a time-domain waveform can be obtained via the inverse Laplace transform as expressed by equ.(11).

$$V_o(s) = \frac{(C_2R_L)s}{C_2^2s^2+(C_2R_L)s+1}V_2(s) \quad (10)$$

$$vo\ (t) = Be^{-bt}(k_3\cosh(w_3t) + k_4\sinh(w_4t)) * v_2(t) \quad (11)$$

Where B, b, k_4, k_5, w_1, and w_2 are defined as follows

$$B = \frac{R_L}{L_2'}; b = \frac{R_L}{2L_2'}; k_4 = 1; k_5 = \frac{\sqrt{C_2}R_L}{2\sqrt{\frac{C_2R_L^2}{4} - L_2'}}; w_1 = w_2 = \frac{\sqrt{\frac{C_2R_L^2}{4} - L_2'}}{\sqrt{C_2}L_2'}$$

The definite solutions for V_1, V_2 and V_0 can be easily obtained when specific elementary values are used. One example is shown in **Table 1** for the capacitive humidity sensor-based system. Here, all the parameter values were based on the real design. R_1 is the internal resistance of the TENG, which is about ~15 kΩ determined by the measurement as is shown later. C_1 is the capacitance of the sensor, which depends on the humidity level and is to be sensed by the sensor system. For the design of the system, the initial humidity is 30 %RH, C_1 is 328 pF as is shown later. For the resonance transmission, the receiving end capacitance C_2 must be equal to the emitter capacitance C_1, i.e. C_2=C_1=328 pF. The inductance value of both the transmitting and the receiving coils L_1, L_2 is set to be 55.5 μH for the frequency required. The diameter of the coils is D=1 cm, the transmission distance is d=10 cm and R_L=300 Ω is the actual value used in the experiment. The mutual inductance coefficient M=1.4 μH is calculated based on equation shown later. The expressive formulas for $V_1(t)$ and $V_0(t)$ are as follows;

$V_1(t)$= $0.0093e^{-(1.5152\times10^5)t}(cos(7.3144\times10^6t) + 1.3354\times10^4\ sin(7.3144\times10^6t) - 0.0093e^{-550t}$

$V_o(t)$=$1.6772\times10^{-8}e^{-550t} - 0.866e^{-3.6496\times10^6t}(cos(6.4790\times10^6t) + 42.6665\ sin(6.4790\times10^6t))$

$+0.0865e^{-1.5152\times10^5t}(cos(7.3411\times10^6t) + 37.1776\ sin(7.3411\times10^6))$

The transmitted signal $V_1(t)$ and the received signal $V_0(t)$ can be calculated with the results shown in **Fig. 2c&d** for this humidity sensor system. From the figure, it is clear that an oscillating signal is generated using the pulsed voltage output from the TENG, consistent with the experimental observation. The oscillating signal received by the receiver has the same resonant frequency as that of the transmitted one with a much-reduced amplitude due to the loss in air and the Ohmic loss via the resistances of the coils and other parasitic ones. It is clear

that the equivalent circuit can reproduce the signals of the L_1C_1 resonant circuit and the receiver terminal respectively, indicating our equivalent circuit model and the analytic formulas are correct and accurate, and can be simply used for designing this type of TENG-based self-powered wireless sensor systems.

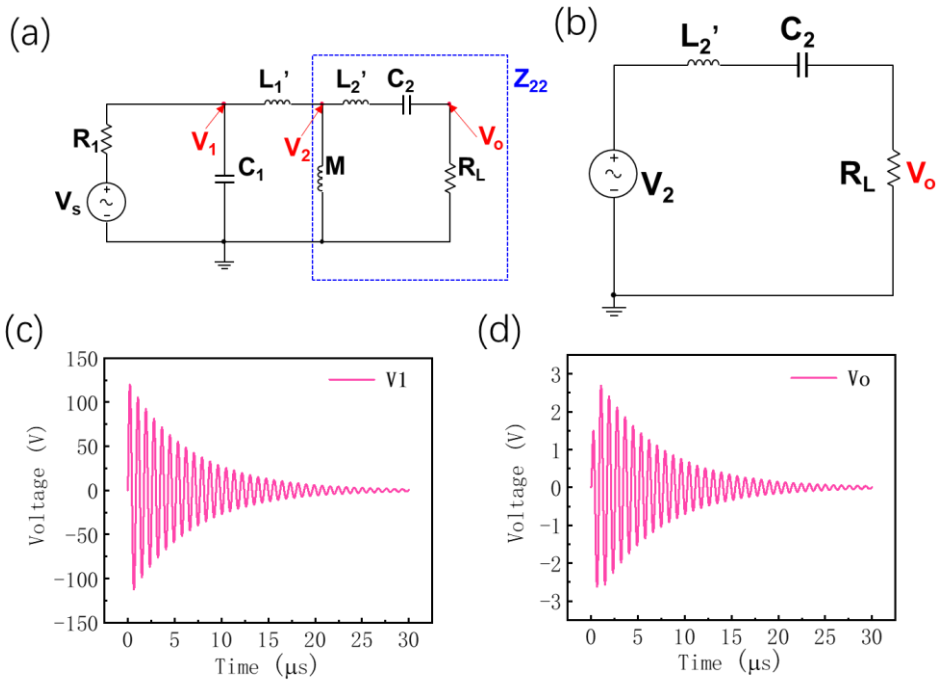

Fig. 2. (a) T-type equivalent circuit for the TENG-based wireless sensor system, V_{TENG} is the output voltage signal of TENG, (b) Simplified equivalent circuit of the WS-TENG receiver, (c) and (d) are the calculated transmitting waveform (V_1) and receive waveform (V_o) of the sensor system, respectively.

Table 1: parameters of the wireless sensor system.

Capacitance C_1	Variable
Capacitance C_2	328 pF
Transmission distance, d	10 cm
Diameter of coil 1, D	1 cm
Diameter of coil 2, D	1 cm
Inductance L_1	55.5 μH
Inductance L_2	55.5 μH
Load R_L	300 Ω
R_1	15 kΩ
Mutual inductance M	1.4 μH
Coil type	Magnetic core

2.3 Performance of PA66 /FEP tribo-materials based TENG

As pointed out by our previous work [29, 30], TENG with higher voltage output is

advantageous for this type of wireless sensor systems with longer transmission distance. To realize a long-distance transmission, it is necessary to utilize high-performance TENG [39, 40]. In this work, we utilized a high-performance TENG for this sensor system by using commercially available fluorinated ethylene propylene (FEP) composite as the negative triboelectric material and nylon-66 (PA66) as the positive triboelectric material. A diode (1N4007) was connected between the aluminum electrodes of the two tribo-plates, which enables electrons to flow back to the metal electrode when the synchronized microswitch is used in the TENG [35].

The contact-separation mode TENG was utilized for this work, the device configuration and the photo image of the TENG device are shown in **Fig. 3a**. The FEP film has a thickness of 100 μm and is glued on the surface of an acrylic support layer by a double-adhesive aluminum tape with a thickness of 100 μm to form the negative tribo-plate. The PA66 membrane has a thickness of 200 μm, and is also adhered on a double-adhesive aluminum tape as the positive tribo-material fixed on an acrylic support layer. The active device area of the triboelectric nanogenerator is 5×5 cm^2. Detailed fabrication process and device structure can be found in Method.

Fig. 3b show the working principle of the TENG. When the two tribo-plates of the TENG is contacted, the microswitch is open and electrons flow from the FEP terminal to the PA66 terminal through the diode. At the separating stage, the circuit is open and the potential between the two tribo-plates increases with the separation distance due to accumulated charges on the surfaces of the tribo-materials that can't flow through the reversely connected diode. When the separation distance reaches the maximum, the microswitch is closed and electrons flow from the FPE plate to PA66 plate through the external circuit with a load instantaneously.

Without the microswitch, the TENG has a typical peak output voltage of 910 V when it is operated under a force of 50 N, a frequency of 2 Hz, and a spacer of 4 mm as shown in **Fig. 3c.** The energy harvested is about 105 μJ/cycle at this condition. The device was tested under various load resistances, the corresponding voltage outputs are summarized in **Fig. 3d**. which also shows the instantaneous power output as a function of load resistance, where the power was calculated by $P=U^2/R$. The maximum peak power reaches 12 mW, corresponding to a peak power density of 4.8 W/m^2, at the match load of ~50 MΩ. More characterization results can be found in Supplementary Information (SI), **Fig. S1**. We found that pre-friction can be used to inject charge into PA66 and FEP to enhance the TENG performance significantly, with the maximum output voltage increased from 910 V to 1700 V. Details about the charge injection into PA66 and FEP are presented in section 2 and Fig.S2 in SI. To clearly demonstrate the

magnificent role of the microswitch in the sensor system, the charge injection was not used in the following experiments. If both the pre-friction charge injection and microswitch were used, it simply generated high voltages >>2500 V, which led to ionization of air between the two triboplates, resulting in unstable TENG performance and unclear understanding of the microswitch role.

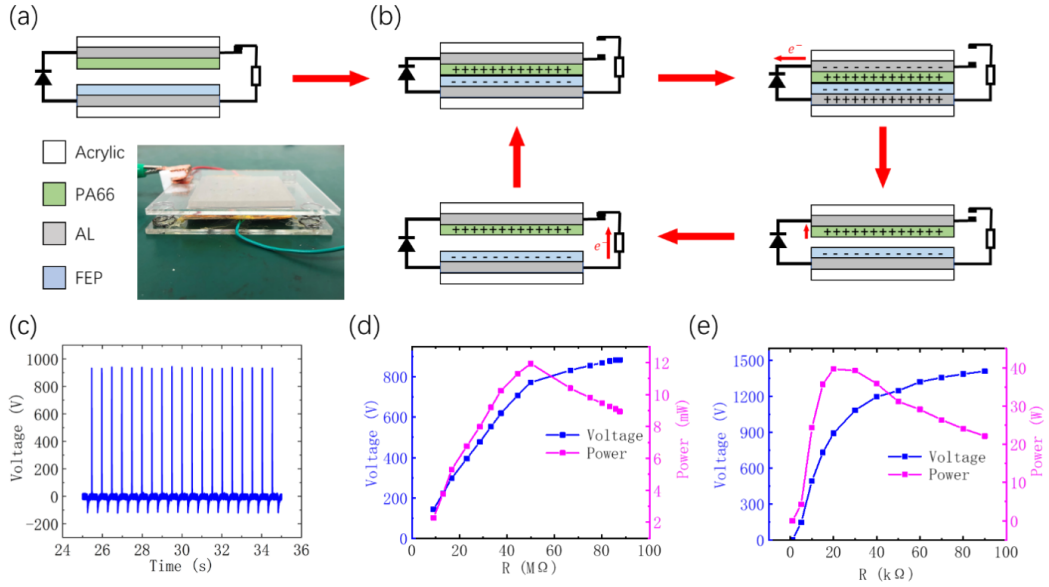

Fig. 3(a) High-performance TENG device structure and a photo image of the TENG, (b) the operating sequences of the TENG. (c) The voltage output of the TENG without microswitch under a force of 50 N, a frequency of 2Hz, and a spacer of 4mm; (d) The output voltage and peak power of the TENG under different loads; and (e) The voltage and peak power output of the TENG with a microswitch integrated as a function of load resistance.

The large internal resistance makes the TENG difficult to match input impedance of the external circuit directly, particularly the resonant circuit used in this sensor system, whose impedance is typically a few kilohms. To optimize the matching impedance of the TENG device with the resonant circuit of the sensor system and to increase the voltage output, a synchronization microswitch was integrated into the TENG in series connection. By using this synchronic microswitch, the TENG is effectively isolated from the circuit for most of the operation time, and the microswitch is closed only when the top triboelectric plate is returned to the maximum separation distance, then the accumulated charge discharges instantaneously in a much shorter time than that without the microswitch, and results in much higher output voltage and peak power density[30, 35]. This is particularly advantageous to maximize the output power to the resonant circuit.

Fig. 3e shows dependence of the voltage and peak power output on load resistance for the

TENG integrated with a microswitch. The match resistance of the TENG outputs has been successfully reduced from 50 MΩ to about 15 kΩ, the output voltage increased to about 1400 V, and the instantaneous peak power reached 40 W, corresponding to a peak power density of 16000 W/m^2, much higher than that of the TENG without the microswitch. Moreover, with the much-reduced match load resistance, this TENG can be connected with the resonant circuit with a maximum power input for the resonant circuit, hence making the wireless sensor system working with high efficiency and relatively longer transmission distance. It should be pointed out that the harvested energy would be similar for both the TENGs with and without the microswitch, the very large voltage and peak power outputs are attributed to the very-short discharging time for the same amount of charges.

2.4 Humidity response of the wireless sensor system

A capacitive humidity sensing experiment was conducted to demonstrate the wireless sensing capability of the sensor system. The humidity sensor used in this work is a commercially available capacitive sensor HS1101. To increase the capacitance range of the humidity sensor and the capacitance variation upon the humidity change, two sensors are connected in parallel here as shown in **Fig. 4a**, with a total capacitance of about 328 pF at 30 %RH (this was used for the equivalent circuit simulation, Table 1). The configuration of the sensor system is schematically shown in **Fig. 1a**, with the humidity sensor located at the C_1 position to form the wireless sensor system. The humidity sensor was placed in a hermetic box and its humidity was controlled by varying the flow ratio of dry N_2 and wet N_2 into the box.

The capacitive humidity sensor was fixed in the humidity-controlled box and the capacitance response of the sensor was characterized under various humidity. **Fig. 4(b)** shows the capacitance value of the sensor as a function of humidity, which varies in the range between 321 to 364 pF when the humidity is in the range of 20 %RH – 80 %RH. As it can be seen that the capacitance of the sensor is linearly correlated to humidity for the humidity range measured.

The oscillating frequency of the signal of the transmitter is determined by[30],

$$f = \frac{1}{2\pi\sqrt{L_1(C_1+C_{TENG})}} \tag{12}$$

Here C_1 is the capacitance of the sensor, C_{TENG} is the capacitance of the TENG when the separation distance of the two plates is at the maximum distance, i.e. 4 mm in this work, and L_1 is the inductance of the coil with a value of 55 μH (magnetic core, 1 cm diameter). The sensor system was designed initially based on a capacitance value of C_1=328 pF for the humidity sensor at a humidity level of 30 %RH. With the circuit parameters shown in Table 1,

the resonant frequency of the transmitter can be calculated to be 1.13 MHz. **Fig. 4c** is a comparison of the generated oscillating signal of the experimental result and theoretical calculation using the derived formulas above at the humidity of 30 %RH, demonstrated excellent agreement between them, again indicating the accuracy of this analytical model and formulas. Fast Fourier transfer (FFT) analysis was then used to analyze the spectra of the signals to identify the resonant frequencies at different humidity levels with the result shown in **Fig. 4d**. When the humidity varies, the sensor capacitance changes and the resonant frequency of the oscillating signal varies in turn, which can be detected by the receiver in distance, realizing instantaneous wireless sensing. With humidity rising, the resonant frequency shifts to low values due to the increased capacitance of the sensor, and the dependence of the resonant frequency of the transmitter on humidity is summarized in **Fig. 4b** by the pink colored dots and line, showing a good linearity for the humidity range measured.

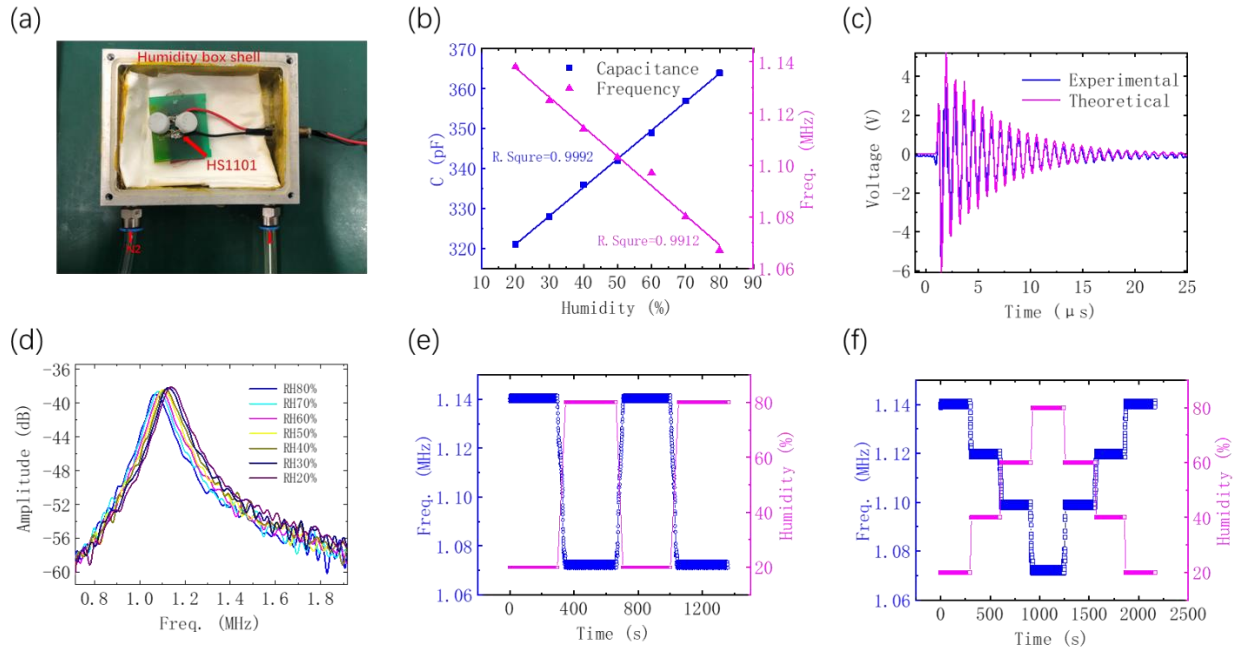

Fig. 4. (a) A photo image of the humidity sensor installed in the hermetic box for humidity sensing, (b) the capacitance value of the humidity sensor and resonant frequency of the sensor system as a function of humidity, (c) comparison of the theoretically calculated oscillating signal with a damped amplitude and the experimental result at the humidity of 30 %RH, which shows an excellent agreement between them, (d) The FFT spectra of the received signals at various humidity levels, (e) humidity response of the wireless humidity sensor system to cyclic change of humidity, and (f) humidity response of the wireless humidity sensor system to step change of humidity.

Fig. 4e shows the response of the humidity sensor system when the humidity is varied cyclically. With the humidity changes back and forth from 20 %RH to 80 %RH, the resonant

frequency of the receiver of the sensor system also changes accordingly. The response time of the sensor system is fast, in a few seconds limited by the humidity sensor itself, which is sufficiently fast for continuous monitoring of environmental humidity. **Fig. 4f** shows the responses of the sensor system to a step variation of humidity, the response of the frequency is instantaneous and stable. Both of the results demonstrate the excellent stability and repeatability of humidity sensing and its instantaneous wireless sensing capability.

2.5 Effect of TENG device size on sensor response

As shown by equ.(12), the oscillating frequency of the sensor system is dependent on the capacitance of the sensor and that of the TENG when the microswitch is closed. Under the conditions of **Table 1**, the effect of TENG size on the performance of the sensor system was investigated with the results shown in **Fig. 5a&b** with the same capacitive sensor and humidity. The maximum amplitude, V_{PP}, of the oscillating signal at the receiver side is magnified by about 2.5 times from ~6 V to ~14 V when the tribo-plate active area increases from 2×2 cm^2 to 8×8 cm^2 with a fixed transmission distance of 10 cm. It can be seen that the larger the plate, the greater the amplitude of the received signal. This is beneficial for the longer distance transmission of sensing information. The significant improvement of the signal amplitude is attributed to the increased amount of charges which is proportional to the tribo-plate area as indicated by equ.(1). The effects of the device size on the oscillating frequency of the system was also investigated. The FFT power spectra of the signals with different tribo-plate areas are shown in **Fig. 5b**. The amplitude increases with active area of the TENG, showing that the larger the plate, the longer the signal transmission distance. Moreover, it can be seen that the resonant frequency decreases with the increase in tribo-plate size as expected from equ.(12). But this effect can be controlled and designed by using known dimensions of tribo-plates, which allows precise calculation of the value of C_{TENG} and determination of the resonant frequency during design. The frequency variation of the sensor system with humidity change of these three different size TENGs is shown in **Fig. 5c**, all of them show good linearity for the humidity level measured. The sensitivity of the humidity sensor is defined as,

$$S = \Delta f/\Delta H \tag{13}$$

Here Δf is the frequency shift, and ΔH is the change of the relative humidity. From **Fig. 5c**, the sensitivity of the wireless humidity sensor can be calculated to be about 1.26 kHz/%RH, and it remains constant for TENGs with different sizes, though the initial resonant frequency decreases with the increase of TENG size due to the increased capacitance.

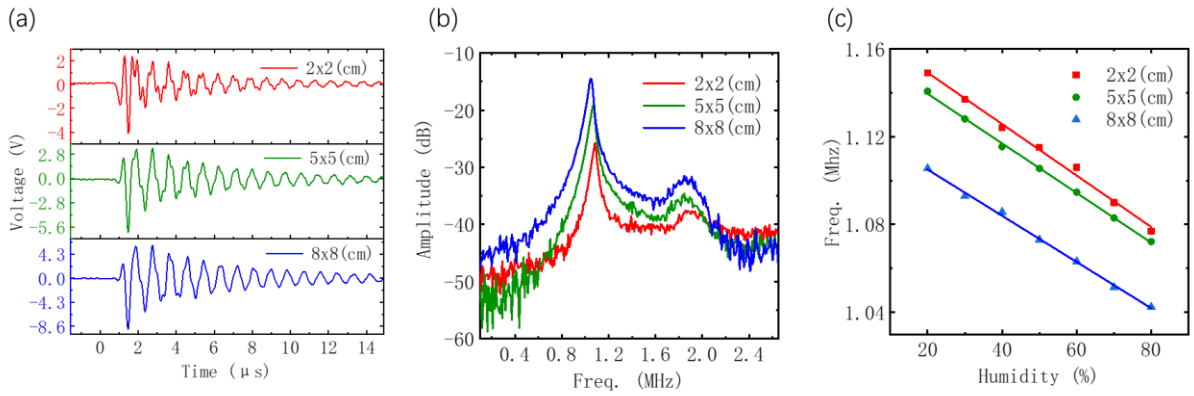

Fig. 5. (a) Time domain transmitted signals of the sensor system with different TENG sizes, with the increase of TENG size, the amplitude of transmitted signal increases, (b) the FFT spectra of the transmitted signals with different TENG sizes, the resonant frequency down-shifted slightly with the increase of TENG size, and (c) dependence of the resonant frequency of the sensor system on humidity with the TENG size as a variable, all of them showed excellent linearity.

2.6 Influence of coil inductor on wireless sensing

The radius of the transmitting and receiving coils, and the distance between the coils have a great influence on the transmission signals. The relevant variable is the coupling coefficient, *k*, of the coils, which can be expressed by the following formula.[30]

$$k = \frac{M}{\sqrt{L_1 L_2}} \tag{14}$$

M is the mutual inductance of the coils. For the selected coils, the inductance values L_1 and L_2 are constants, and the only variable is the mutual inductance M of the coils. The value of M is determined by the geometry, diameter and the number of turns of the coils, and the mutual position between the coils, and is independent of the current in the coils. The mutual inductance, M, of the coils can be obtained by equ.(15)[41],

$$M = \frac{\mu_0 i}{4\pi} \oint_1 \oint_2 \frac{dl_1 \cdot dl_2}{r_{12}} \tag{15}$$

where *i* is the magnitude of the current in the first coil, *dl* is an element of the coil and r_{12} is the distance from the element dl_1 to the element dl_2[41]. Once the mutual inductance value is obtained, then the mutual inductance coefficient, *k*, can be calculated based on equ.(14).

For better and longer distance signal transmission, large coils were used in our previous work[30]. In this work, a pair of 1cm coils with a magnetic core was used to improve the transmission distance (d), so that to reduce the dimension of the system. The 1cm and 20 cm air-core coils were also used to compare the signal transmission ability. **Fig. 5a** shows the normalized coupling coefficient, *k,* as a function of distance (d) for the three types of

transmission coils. For all the coils, the normalized coupling coefficients decrease drastically as the transmission distance increases. As shown in the figure, the normalized coupling coefficient of the magnetic core coils is much larger than that of the air-core coils with the same diameter.

The coupling coefficients of the air-core coils decrease quickly with the distance compared with that of the magnetic-core coil, and the transmission signal becomes so weak for the 1cm diameter air-core coils at a distance about d=10 cm merely, it is not possible to obtain measurable signal. Whereas the transmission signal for the 20 cm diameter air-core coils at the same distance is relatively stronger because of the larger diameter of the coil. On the other hand, for the sensor system with a pair of 1cm diameter magnetic core coils, the coupling efficient becomes much stronger, about two orders of magnitudes larger compared with that of the 1cm diameter air-core coils. **Fig. 5b** is the filtered signal of different diameter air-core coils at the same coil distance of 10 cm, shows that the signal amplitude, V_{PP} ~8 V, received by the 20 cm diameter air-core coil is much greater than that (V_{PP} ~0.1 V) by the 1cm diameter air-core coil. It indicates that the system with larger diameter coils is able to transmit signal for longer distance. The 20 cm air-core coil can transmit the sensing signals up to 90 cm (d/D=4.5) as shown in **Fig. 5c**.

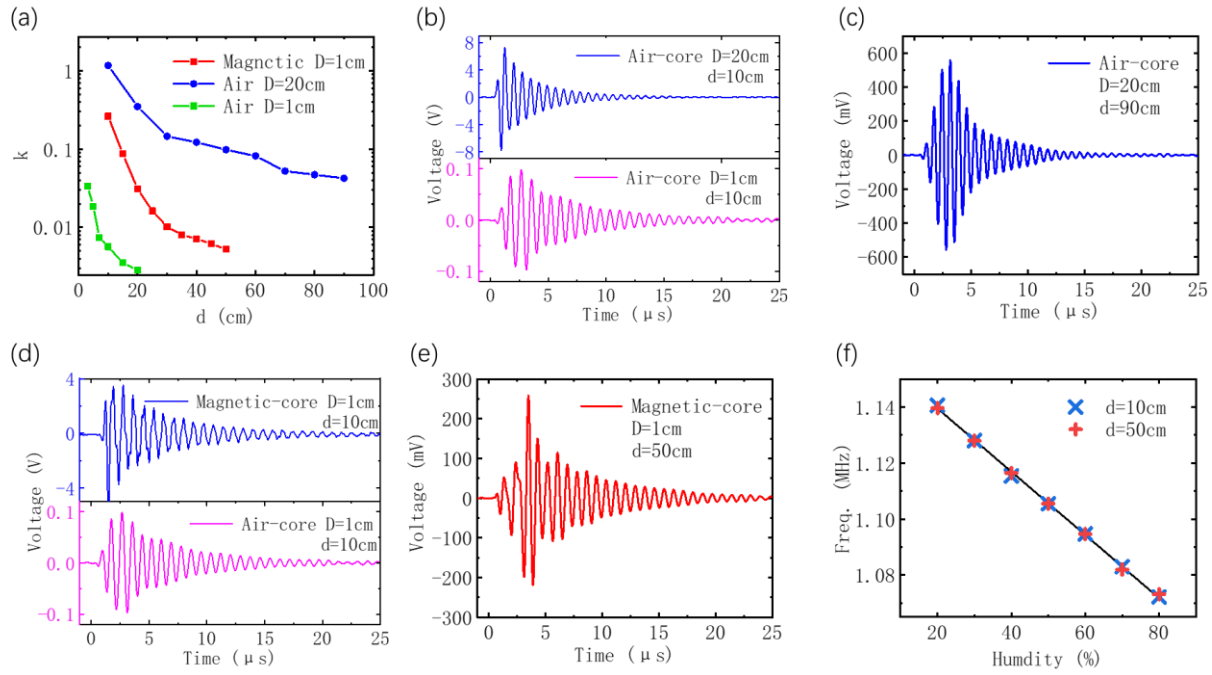

Fig. 6. (a) Coupling coefficients as a function of distance for the magnetic-core coils with a diameter of 1 cm and the air-core coils with diameter of 1 cm and 20 cm respectively. (b) is the comparison of filtered signals of different diameter air-core coils at the same distance (d = 10 cm), (c) is the received signal of the 20 cm air-core coils at distance of 90 cm, (d) is the comparison of filtered signals of

different types of coils (magnetic-core and air-core) with the same diameter at the distance of 10 cm, (e) is the transmission signal of the 1 cm magnetic-core coil sat distance of 50 cm, (f) is resonant frequency of the received signal as a function of humidity by the 1 cm magnetic-core coils at the distance of 10 cm and 50 cm respectively. Although the signal amplitude decreases significantly for the distance of 50 cm, the resonant frequency remains unchanged.

Although increasing the coil diameter could increase the transmission distance, it will make the sensing system larger, not good for application. To increase the transmission distance without increasing the dimension of the sensor system, utilization of magnetic core coils would be a good solution. **Fig. 5d** is the comparison of the filtered signals of different types of coils (magnetic-core and air-core) with the same diameter (D=1 cm) at the same transmission distance (d=10 cm). This clearly shows that, at the same transmission distance and the same coil diameter, the signal amplitude transmitted by the magnetic coils is much greater than the air-core coil. For the magnetic-core coils with 1cm diameter, the system can transmit signals up to 50 cm (d/D=50) as shown in **Fig. 5e**, with the amplitude of V_{PP} ~250 mV, sufficiently large for electronic device to sense and process. The results indicate that the magnetic core of the coils can improve the wireless transmission capability of the sensing system significantly. It should be pointed out that there is a high frequency component in the received signals due to the parasitic capacitance and inductance, which can be eliminated either by careful tuning of the circuit or using a filter to remove it at the signal processing stage as schematically explained in **Fig. S3** in SI.

Fig. 5f is the wireless humidity response received by the 1 cm magnetic-core coils at the distances of 10 cm and 50 cm respectively. The resonant frequency of the signals received at different distances remains unchanged though the amplitude becomes smaller as the coil distance increases. This result further indicates the feasibility of long-distance wireless sensing of the sensor system. The setup for these two sensor systems with 1 cm magnetic core coils and 20 cm air-core coils respectively are shown in **Fig. S4** in SI for clarity, clearly show the much-reduced diameter of the sensor system. Obviously, using a magnetic core coil or increasing the diameter of the coil can increase the signal transmission distance. When the coil diameter is 1 cm, the transmission distance of the magnetic-core coil is more than five times longer than that of the air-core coil. If a larger diameter magnetic-core coil is used, then the signal transmission distance can be increased to about 5 meters.

3. Conclusions

In this work, a TENG-based self-powered wireless and chipless sensor system has been proposed and demonstrated with a capacitive humidity sensor. A mathematical model and equivalent circuit have been developed for the sensor system with general implication. Analytical solutions have been derived for the voltage output received by the receiver terminal. A high-performance TENG integrated with a synchronization microswitch for impedance match with the resonant circuit was fabricated and assessed using PA66 and FEP as the positive and negative triboelectric materials respectively. The maximum output peak voltage and the peak power density of this TENG with the microswitch reached 1400 V and 16000 W/cm^2 respectively. The TENG-based self-powered wireless humidity sensor system was designed and characterized. The sensor system possesses a fast response speed with stable and repeatable responses to humidity changes, and has a good linearity for the humidity level assessed, with a sensitivity of ~1.26 kHz/%RH. Furthermore, by using magnetic-core coils with a diameter of 1 cm, the transmission distance of the sensor system can reach up to 50 cm. The use of magnetic core coils significantly reduces the dimensions of the sensor system and increases the wireless sensing distance, beneficial for widespread application of this type of sensor systems. This work has demonstrated the feasibility of the self-powered instantaneous wireless and chipless sensor system with excellent capability for application.

4. Methods

4.1 Fabrication of TENG

The sensor system is shown in **Fig. 1(a)**, which consists of a TENG, magnetic resonance-coupled wireless transmission device, and a capacitive humidity sensor. The TENG was fabricated using fluorinated ethylene propylene (FEP) membrane as the negative triboelectric material and nylon-66 (PA66) as the positive triboelectric material. The FEP film with a thickness of 100 μm was purchased from Dupont. It was cut into a square of 5×5 cm^2 and glued on the surface of a commercial acrylic support layer by a double-adhesive aluminum tape to form the negative tribo-plate. The PA66 membrane with a thickness of 200 μm was purchased from Dupont, and similarly was cut into a square of 5×5 cm^2 and glued on the surface of an acrylic plate by a double-adhesive aluminum tape to form the positive tribo-plate. The schematic diagram of the fabrication process is shown in **Fig. S5** in SI.

4..2 Characterization instruments

A linear motor (H01-48 × 250) was utilized to control the cyclic contact force, frequency, and distance, which is able to control the force, contacting frequency, and traveling distance. The output voltages of the TENG were measured using an oscilloscope (Tektronix MDO3022). The capacitive humidity sensor HS1101 was placed in a hermetic box with two through-holes for humidity N_2 gas to pass through for humidity sensing. The relative humidity in the box was controlled by changing the flow ratio of dry N_2 and wet N_2 into the box, while keeping the total flow rate at a constant value of 500 sccm. A hygrometer (TASI-621) was used to monitor the humidity in the box. The schematic diagram of the setup for humidity sensing is shown in **Fig. S6** in SI.

Acknowledgement:

This work was funded by National Key R&D Program of China (No.2018YFB2002500，2018YFA0701400，2018YFC0809200), National Natural Science Foundation of China (No. 61801158, 61974037, 61904042, 61827806), NSFC-Zhejiang Joint Fund for the Integration of Industrialization and information(No.U1909212). Zhejiang Province Key R & D programs (No.2020C03039，2021C05004，2021C03062，2021C03108)

References

[1] J. Gubbi, R. Buyya, S. Marusic, M. Palaniswami, Future Generation Computer Systems, 29(2013) 1645-1660.

[2] D. Silver, A. Huang, C. J. Maddison, A. Guez, L. Sifre, G. van den Driessche, J. Schrittwieser, I. Antonoglou, V. Panneershelvam, M. Lanctot, S. Dieleman, D. Grewe, J. Nham, N. Kalchbrenner, I. Sutskever, T. Lillicrap, M. Leach, K. Kavukcuoglu, T. Graepel, D. Hassabis, Nature, 529(2016) 484-489.

[3] A. Somov, A. Baranov, A. Savkin, D. Spirjakin, A. Spirjakin, R. Passerone, Sensors and Actuators A: Physical, 171(2011) 398-405.

[4] A. Rghioui, Automation, Control and Intelligent Systems, 5(2017) 83.

[5] M. F. Farooqui, M. A. Karimi, K. N. Salama, A. Shamim, Advanced Materials Technologies, 2(2017) 1700051.

[6] Y. Chen, Y.-C. Wang, Y. Zhang, H. Zou, Z. Lin, G. Zhang, C. Zou, Z. L. Wang, Advanced Energy Materials, 8(2018) 1802159.

[7] D. Prasad, V. Nath, Microsystem Technologies, 24(2018) 1553-1563.

[8] Z. Duan, Y. Jiang, M. Yan, S. Wang, Z. Yuan, Q. Zhao, P. Sun, G. Xie, X. Du, H. Tai, ACS Applied Materials & Interfaces, 11(2019) 21840-21849.

[9] N. Afshar-Mohajer, C. Zuidema, S. Sousan, L. Hallett, M. Tatum, A. M. Rule, G. Thomas, T. M. Peters, K. Koehler, J Occup Env Hyg, 15(2018) 87-98.
[10] M. P. Da Cunha, R. Lad, P. Davulis, A. Canabal, T. Moonlight, S. Moulzolf, D. Frankel, T. Pollard, D. McCann, E. Dudzik, Wireless acoustic wave sensors and systems for harsh environment applications, 2011 IEEE Topical Conference on Wireless Sensors and Sensor Networks, IEEE2011, pp. 41-44.
[11] J. Chen, S. Kher, A. Somani, Distributed fault detection of wireless sensor networks, Proceedings of the 2006 workshop on Dependability issues in wireless ad hoc networks and sensor networks2006, pp. 65-72.
[12] Q. Tan, T. Luo, T. Wei, J. Liu, L. Lin, J. Xiong, Journal of Microelectromechanical Systems, 26(2017) 351-356.
[13] S. F. Shaikh, M. M. Hussain, Applied Physics Letters, 117(2020) 074101.
[14] H. Kou, Q. Tan, Y. Wang, G. Zhang, S. Su, J. Xiong, Sensors and Actuators B: Chemical, 311(2020) 127907.
[15] S. Rodríguez, T. Gualotuña, C. Grilo, Procedia Computer Science, 121(2017) 306-313.
[16] S. Ankanahalli Shankaregowda, R. F. Sagade Muktar Ahmed, C. B. Nanjegowda, J. Wang, S. Guan, M. Puttaswamy, A. Amini, Y. Zhang, D. Kong, K. Sannathammegowda, F. Wang, C. Cheng, Nano Energy, 66(2019) 104141.
[17] Y. Yang, Y. S. Zhou, H. Zhang, Y. Liu, S. Lee, Z. L. Wang, Adv Mater, 25(2013) 6594-6601.
[18] E. Sardini, M. Serpelloni, IEEE Trans Instrum Meas, 60(2011) 1838-1844.
[19] J. Qian, X. Jing, Nano Energy, 52(2018) 78-87.
[20] D. Dondi, A. Bertacchini, D. Brunelli, L. Larcher, L. Benini, IEEE Transactions on Industrial Electronics, 55(2008) 2759-2766.
[21] K. Opasjumruskit, T. Thanthipwan, O. Sathusen, P. Sirinamarattana, P. Gadmanee, E. Pootarapan, N. Wongkomet, A. Thanachayanont, M. Thamsirianunt, IEEE Pervasive computing, 5(2006) 54-61.
[22] Y. J. Kim, H. M. Gu, C. S. Kim, H. Choi, G. Lee, S. Kim, K. K. Yi, S. G. Lee, B. J. Cho, Energy, 162(2018) 526-533.
[23] X. Tang, X. Wang, R. Cattley, F. Gu, A. D. Ball, Sensors, 18(2018) 4113.
[24] L. Jin, W. Deng, Y. Su, Z. Xu, H. Meng, B. Wang, H. Zhang, B. Zhang, L. Zhang, X. Xiao, M. Zhu, W. Yang, Nano Energy, 38(2017) 185-192.
[25] Y. Wu, Y. Hu, Z. Huang, C. Lee, F. Wang, Sensors and Actuators A: Physical, 271(2018) 364-372.
[26] Y. Shi, Y. Wang, Y. Deng, H. Gao, Z. Lin, W. Zhu, H. Ye, Energy Convers Manage, 80(2014) 110-116.
[27] Q. Zheng, H. Zhang, B. Shi, X. Xue, Z. Liu, Y. Jin, Y. Ma, Y. Zou, X. Wang, Z. An, W. Tang, W. Zhang, F. Yang, Y. Liu, X. Lang, Z. Xu, Z. Li, Z. L. Wang, ACS Nano, 10(2016) 6510-6518.
[28] M. Bobinger, S. Keddis, S. Hinterleuthner, M. Becherer, F. Kluge, N. Schwesinger, J. F. Salmeron, P. Lugli, A. Rivadeneyra, IEEE Sens J, 19(2019) 1114-1126.
[29] J. Chen, W. Xuan, P. Zhao, U. Farooq, P. Ding, W. Yin, H. Jin, X. Wang, Y. Fu, S. Dong,

J. Luo, Nano Energy, 51(2018) 1-9.
[30] C. Zhang, J. Chen, W. Xuan, S. Huang, B. You, W. Li, L. Sun, H. Jin, X. Wang, S. Dong, Nature Communications, 11(2020) 1-10.
[31] F. R. Fan, L. Lin, G. Zhu, W. Wu, R. Zhang, Z. L. Wang, Nano Lett, 12(2012) 3109-3114.
[32] F.-R. Fan, Z.-Q. Tian, Z. Lin Wang, Nano Energy, 1(2012) 328-334.
[33] S. Lee, Y. Lee, D. Kim, Y. Yang, L. Lin, Z.-H. Lin, W. Hwang, Z. L. Wang, Nano Energy, 2(2013) 1113-1120.
[34] J. Zhong, Q. Zhong, F. Fan, Y. Zhang, S. Wang, B. Hu, Z. L. Wang, J. Zhou, Nano Energy, 2(2013) 491-497.
[35] G. Cheng, Z.-H. Lin, L. Lin, Z.-l. Du, Z. L. Wang, Acs Nano, 7(2013) 7383-7391.
[36] P. Vasandani, B. Gattu, Z.-H. Mao, W. Jia, M. Sun, Nano Energy, 43(2018) 210-218.
[37] S. Niu, S. Wang, L. Lin, Y. Liu, Y. S. Zhou, Y. Hu, Z. L. Wang, Energy Environ Sci, 6(2013) 3576-3583.
[38] S. Niu, Z. L. Wang, Nano Energy, 14(2015) 161-192.
[39] K. Xia, H. Tang, J. Fu, Y. Tian, Z. Xu, J. Lu, Z. Zhu, Nano Energy, 67(2020) 104259.
[40] J. Wang, K. Xia, J. liu, T. Li, X. Zhao, B. Shu, H. Li, J. Guo, M. Yu, W. Tang, Z. Zhu, Nano Energy, 69(2020) 104461.
[41] F. Flack, E. James, D. Schlapp, Med Biol Eng, 9(1971) 79–85.

Supplementary Information

Fully self-powered instantaneous wireless humidity sensing system based on triboelectric nanogenerator

Liangquan Xu,[1] Weipeng Xuan,[1] Jinkai Chen,[1]Chi Zhang,[1] Yuzhi Tang,[1] Xiwei Huang,[1] Wenjun Li,[1] Hao Jin, [2] Shurong Dong,[2] Wuliang Yin,[3] Yongqing Fu,[4] Jikui Luo[2,1]

1. Characteristics of TENG

Fig. S1a shows the peak voltage output of the TENG as a function of force applied, which increases with the increase of force continuously, because of the increased friction between the two tribo-materials with the increased force, as well as the surface charge density of the tribo-materials. The TENG was used to charge a 100 μF capacitor using a standard bridge type rectification circuit, and voltage of the capacitor increases rapidly and reaches up to 50 V in about 20 sec as shown in **Fig. S1b**, demonstrating the superior performance of the TENG.

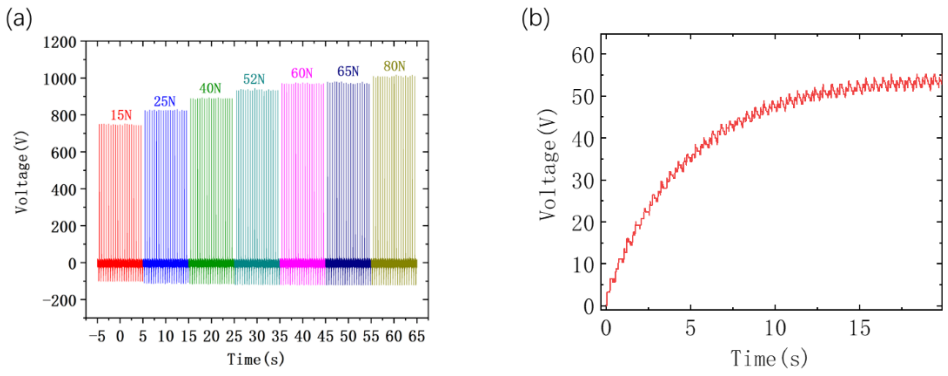

Fig. S1. (a) is the output voltage of the TENG as a function of force applied, and (b) is the voltage of a 100 μF capacitor as a function of charging time when the TENG is used to charge the capacitor.

2. Charge injection by pre-friction to enhance performance of the TENG

Charge injection was found to increase the surface charge density, hence enhance performace of TENG which can be achieved by pre-rub the tribo-plates used for the TENG fabrication in this work. If positive triboplate is rubbed with other negative materials, it makes the positive triboplate lose some electrons in advance. Similarly, tif he negative triboplate is rubbed with other positive materials to gain some electrons in advance. When they are assembled into TENG and operated under periodic pressure, the positive triboplate and

negative triboplate with pre-friction in advance will lose and gain more electron. Therefore, the electric potential difference between the tribo-plate is increased and the output performance of TENG is improved. In this work, the PA66 was rubbed with PTFE, while the FEP was rubbed with carbon film. The pre-rubbed PA66 and FEP membranes were used as positive triboplate and negative triboplate, respectively, as shown in **Fig. S2(a)**.

Comparison of output signal of TENG with and without charge injection at the same condition is shown in the **Fig.S2(b).** The corresponding voltage and instantaneous power outputs versus various load resistances were investigated for the devices with and without charge injection, with the results shon in **Fig. S2(c)**. It shows that performance of the TENG has been improved significantly. The maximum output voltage is increased from 910 V to 1700 V after charge injection by pre-friction. The maximum peak power reaches 24 mW, corresponding to a peak power density of 9.6 W/m^2, at the match load of ~40 MΩ (Uninjected charge is about ~50MΩ).

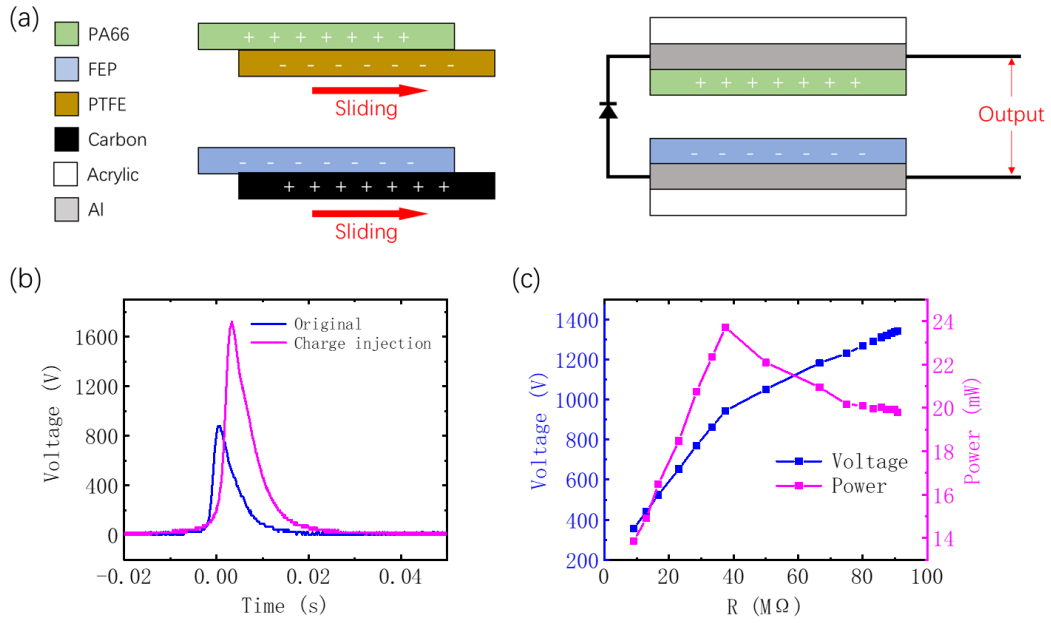

Fig. S2. (a) Schematic diagram of charge injection by pre-rubbing method. (b) Comparison of output signal of TENG with and without charge injection at the same test condition. (c) Output voltage and peak power density of the TENG with charge injection as a function of load.

3. High frequency component on the received signal and filtering

When the receiving circuit receives a signal, the parasitic factors (parasitic capacitance, parasitic inductance, and parasitic resistance) in the circuit will generate an oscillating signal with high-frequencies.[1] **Fig. S3(a)** is a typical receiving circuit received signal. **Fig. S3(b)** is high frequency component part of original signal. High frequency components can be removed with the Chebyshev low pass filter at the receiving terminal, or treated at the signal processing

stage.

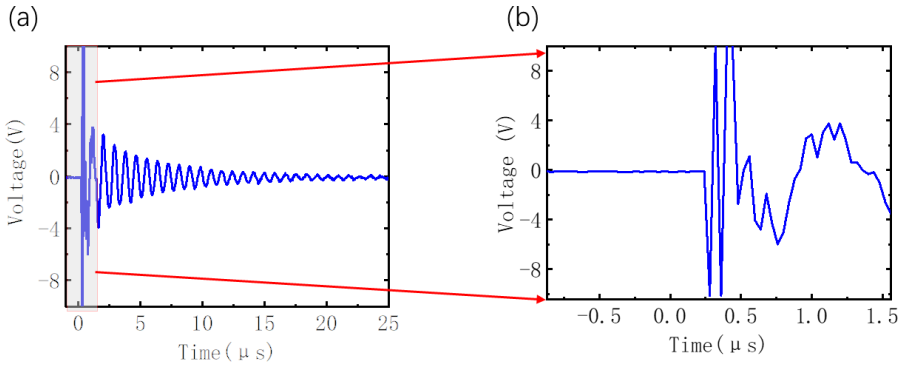

Fig. S3. (a) Typical receiving circuit receives signal. (b) High frequency component part of original signal.

4. Configuration of the wireless sensor system

Fig. S4 shows photos of the wireless humidity sensor systems having a pair of magnetic-core coils with the diameter of 1cm (a) and air-core coils with a diameter of 20 cm (b), respectively.

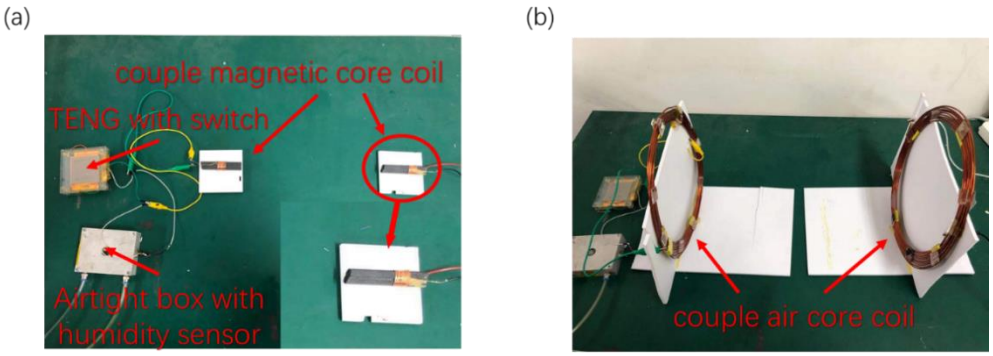

Fig. S4. Photos of the wireless humidity sensor system, (a) having a pair of magnetic-core coils with a diameter of 1cm; and (b) with a pair of air-core coils with a diameter of 20 cm.

5. Fabrication process of TENG

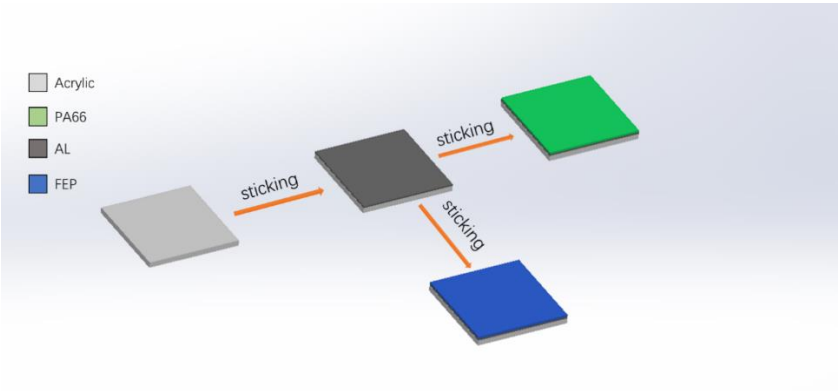

Fig. S5. Schematic diagram of the fabrication process of TENG.

6. Precise control of humidity

The humidity in a hermetic box was controlled by varying the dry N_2 gas to wet N_2 gas ratio into the box. **Fig. S6** shows the schematic diagram of the measurement setup for humidity sensing.

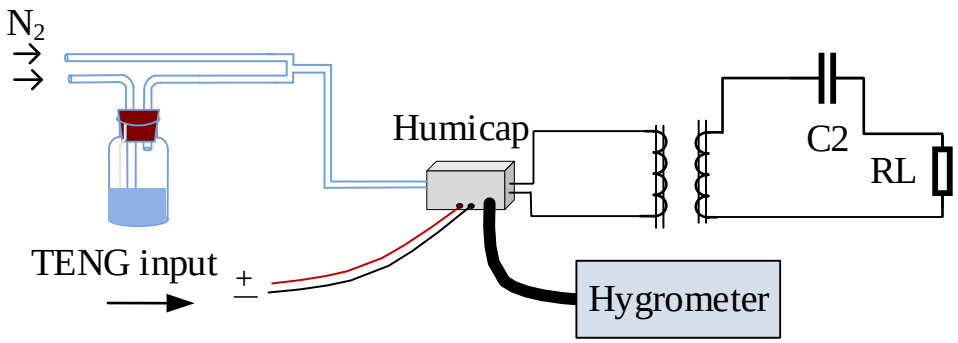

Fig. S6. Schematic diagram of the setup for humidity sensing.

References

[1] C. Zhang, J. Chen, W. Xuan, S. Huang, B. You, W. Li, L. Sun, H. Jin, X. Wang, S. Dong, Nat. Commun., 11(2020) 1-10.